ACTA ACUSTICA UNITED WITH ACUSTICA
Vol. 92 (2006) 826 – 841

Aeroacoustics of the Bullroarer

Michel Roger
École Centrale de Lyon, Laboratoire de Mécanique des Fluides et Acoustique, UMR CNRS 5509,
36 avenue Guy de Collongue, 69134 Ecully, France

Stéphane Aubert
FLUOREM, 64 Chemin des Mouilles, 69130 Ecully, France

Summary
The present paper is about the physical understanding and a complete theoretical modelling of the sounding instrument called bullroarer and used by aboriginal tribesmen. The running of the bullroarer clearly involves aeromechanical aspects, closely related to the process of autorotation, as well as aeroacoustical aspects. Both are investigated here. The mechanical equations are solved in a first step, using a set of two–dimensional unsteady RANS computations as a way to deduce the instantaneous aerodynamic moment and forces. The kinematics and the unsteady forces are used in a second step to calculate the radiated sound field, according to the acoustic analogy. Preliminary theoretical results for the autorotation sound of a rectangular plate in stabilised conditions are found to agree well with measurements performed in an open-jet anechoic wind tunnel. The sound synthesis of a bullroarer based on the physical model is finally shown to fairly reproduce the main features observed in a typical time-frequency analysis.

PACS no. 43.28.R, 43.75.

1. Introduction

The bullroarer is an aeromechanical instrument, which sounds somewhat like the roaring of a bull, this being the origin of the name, or like a propeller with periodic change in pitch and intensity [1]. The oldest known bullroarer is prehistoric and was found in Dordogne (France). The bullroarer was also used in ancient Greece (the French name *rhombe* is derived from the Greek word *rombos*). It is principally found now in various ethnic groups in Oceania, essentially aboriginal tribesmen in Australia, and in South America [2], though still mentioned in many other areas [3, 4]. In most cases, the bullroarer is involved in traditional ceremonies. It has been occasionally introduced in popular music, as a piece of fun or originality, and is commonly sold as a toy for children. A bullroarer can be seen and heard in the movie 'Crocodile Dundee 2'.

A traditional bullroarer is made of a flat plate of wood or bone, less usually metal, with nearly elliptical cross-section, called the slat. It is generally painted or carved with traditional patterns (see Figure 1), and so is often the support of a specific ethnic art. The slat is tied to a string, typically about one meter long, the other end of which is held in one's hand.

The bullroarer is classified as a whirling aerophone [4]. The user drives it on a circular path around his hand, in the same way as a sling or a lasso, either in a vertical plane on his side or in a horizontal one over his head, depending on the string length. When running, the slat experiences a rapid proper rotation around its main axis of inertia, here referred to as the spinning motion. Combined with the relative lateral flow on the slat due to the whirling motion, this results in a periodic vortex shedding, responsible for an intense sound radiation. The mechanism is extensively investigated throughout the paper.

From the ethnical point of view, apart from cultural and/or ritual aspects, the bullroarer, together with the boomerang, indicates a fascinating intuitive perception of fluid dynamics.

From the physical point of view, which is the essential scope of the present paper, it is certainly the simplest device involving complicated and complementary aspects, both aeromechanical and aeroacoustical. In that sense, it deserves a peculiar attention and must be understood as a privileged way to infer fundamental mechanisms which can be determinant in some other situations of technological interest (valves or rotating splitter plates in ducts, for instance), more than simply considered as a picturesque matter of investigation.

The present paper is devoted to a complete theory of the bullroarer, coupling both aeromechanical and aeroacoustical aspects. The theoretical approach is also validated by basic experiments performed in an anechoic chamber with an open jet wind tunnel. A short description of the behaviour of the bullroarer and some ethnological considerations are given in section 2 below. Section 3 deals first with the equations of general mechanics applied to the slat. It is

Received 14 July 2005,
accepted 13 June 2006.

emphasized that the motion is determined by aerodynamic forces and moment, together with the return torque from the string. The acoustical equations are then introduced and the problem is stated in terms of equivalent sources, according to the classical acoustic analogy [5]. The local flow field around the slat is theoretically investigated in section 4, on a simplified configuration where the slat axis is fixed and the whirling motion replaced by an equivalent perpendicular, uniform flow. It is understood that the spinning motion of the bullroarer results from a more general phenomenon called autorotation and well known in fluid dynamics. An experiment dedicated to autorotation is described in section 5, in which the basic aerodynamic and acoustic features are investigated. Finally, the full equations of motion are solved in section 6 and used to propose a complete aeroacoustic model of the sound radiated by a bullroarer.

The whole problem is considered as a synthesis topic, joining mechanics, fluid dynamics and acoustics, which makes the bullroarer a pedagogical example of real interest. It is to be borne in mind that the word proper-rotation or spinning motion is used here to mean the rotation about the main axis of inertia of the slat, whereas autorotation means the ability for a slat with symmetric cross-section to spin when embedded in a flow without external energy supply, according to the definition proposed by Lugt [20]. In other words, autorotation is a special case of spinning motion.

Preliminary results have been previously published by Roger *et al.* [6]. More recently, a similar study has been reported by Fletcher *et al.* [7] on a different theoretical basis.

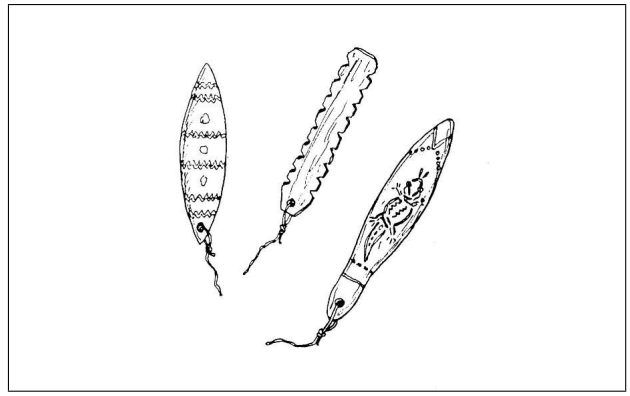

Figure 1. Traditional bullroarers with painted patterns, from [1] and [4].

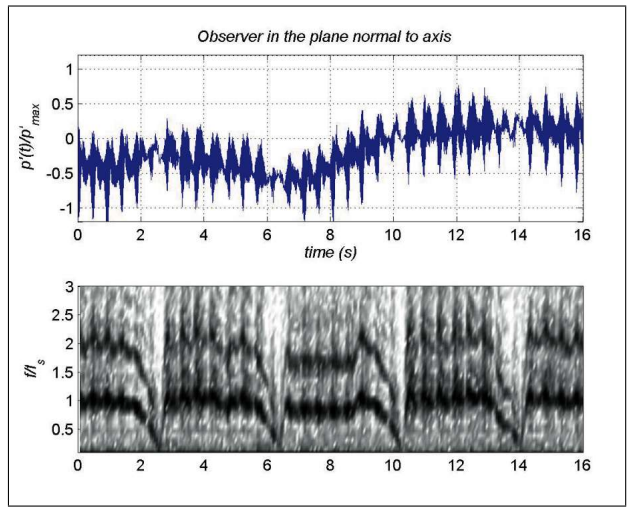

Figure 2. Typical analysis of bullroarer sound, as measured normal to the whirl axis. Top: acoustic pressure signal scaled by its maximum amplitude. Bottom: time-frequency plot; frequency made non-dimensional by the dominant spinning frequency f_s.

2. General Features

As stated in the introduction, the sound radiated by the bullroarer is due to the spinning motion of the slat whirled through the air. As soon as this motion is started, the string is progressively twisted and experiences increasing torsional stress, so that, when a critical value of the return torque exerted by the string is achieved, the proper rotation goes to zero and immediately restarts in the opposite sense. And so on. A periodic inversion of the proper rotation occurs, even with constant whirling frequency. Now any spinning body translating through the air, such as a golf or tennis ball, experiences a mean lift force normal to the direction of motion. This is called the Magnus effect (see for instance Batchelor [8]). As a consequence of this effect on the slat, the string of a bullroarer follows a conical surface instead of rotating in a plane. The aperture of the cone is large in practice and is reversed each time the proper rotation changes. Increasing driving frequency by hand increases pitch as well as intensity of the sound, which is typical of aeroacoustic phenomena. Furthermore, slats with larger chord lengths obviously generate lower frequency sounds. These variations are used by some Amazonian indians to get different sounds by associating large, slow bullroarers to small, fast-running ones, during the same ceremonies [2].

Three chracteristic time scales are involved in the running of the bullroarer:

- the period of the whirl imposed by the user, $T_0 = 2\pi/\Omega_0$; this one will be assumed constant in the present analysis, for simplicity;
- the variable spinning period, $T_s = 2\pi/\Omega$;
- the period of the cycle corresponding to the inversion in proper rotation, determined by the mechanical properties of the string, say T_r.

These time scales are quite different from each other, according to the general relationship $T_r > T_0 \gg T_s$, and help to understand the perceptive features of the bullroarer sound: the instantaneous source frequency $1/T_s$ varies in time, slightly modulated by the driving frequency $1/T_0$. Apart from this, T_r is responsible for additional cyclic variations. A typical sample of bullroarer sound as measured at 90° from the whirl axis in an anechoic room (see section 5 for the details) is shown in Figure 2, where the time signal is displayed at the top and the time-frequency

analysis at the bottom. The averaged value of the fundamental spinning frequency f_s, here around 100 Hz, is used to make the frequency non dimensional. This frequency and its harmonic $2f_s$ dominate the instantaneous tonal behaviour. The cycles of inversion, of about 4 seconds, are clearly identified: the tone frequency exhibits a progressive decrease at the end of each cycle, as the spinning motion decelerates, and a significantly faster increase at the beginning of the next cycle, as the spinning rate suddenly returns to its maximum value. Additional modulations are observed with the imposed whirling period, about 2 revolutions per second in the case of the figure. These are due to physical reasons detailed in section 6 and to the irregular effort made by the driver at each revolution to overcome the aerodynamic drag and sustain the whirling motion.

All these variations make the bullroarer sound very rich and impressive; the resulting wobbling-effect certainly contributes to the feeling experienced by the listeners, especially in the case of a low-pitch bullroarer. This in turn may explain the magical connotation attributed to the bullroarer by tribesmen in most areas of the world where it is found, as well as the use made in other areas to frighten away animals from plantations. Apart from the places where it is considered as a toy or a device of common use, the bullroarer is a sacred object more than a true musical instrument. It is dedicated to initiatic ceremonies and, as such, it appears to be a complicated symbol. In Australia, for instance, it is used when making the young boys enter the manhood condition through sacred rites, or is believed the support of spirit voices. The bullroarer is taboo, women and non-initiated persons not being allowed to see, hear or use it.

It is quite remarkable that a similar quasi supernatural connotation is given the same instrument by different civilizations, such as Amazonian indians and aboriginals for instance. It can be guessed that the particular aforementioned modulations around the basic low-frequency sound are responsible for this. As suggested by Schaeffner [3], a magical significance is associated to the notion of the sounding circle, as the perfect shape; the same holds with some sacred dances. The circular motion induces a hypnotical or obsessional repetitivity, inviting people to a kind of madness, in the sense of a communication with the spirits of ancients.

Ethnology is not the matter of the present paper, however. For more information, the reader may refer to Schaeffner [3] and to the list of references given in Sadie [4]. Nevertheless, the psychoacoustic features of the bullroarer are surely unique. The purpose of this paper is to try and reproduce correctly the major mechanisms involved in the bullroarer expressiveness, so that the model can be used to perform realistic sound synthesis.

3. Theoretical formulation

3.1. Mechanical Equations of Motion

In order to emphasize the main features of interest while discarding secondary ones, the bullroarer is considered to

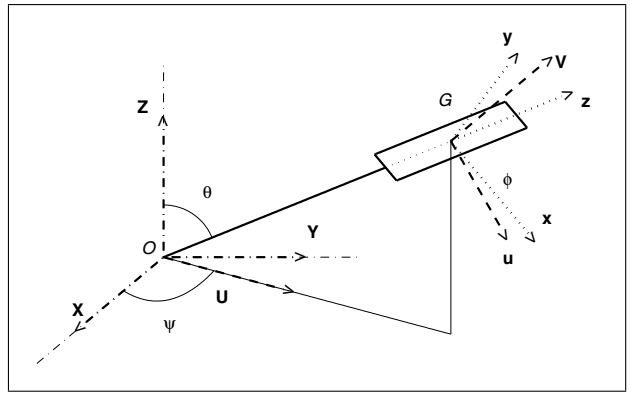

Figure 3. Systems of coordinates for the analysis of the bullroarer kinematics.

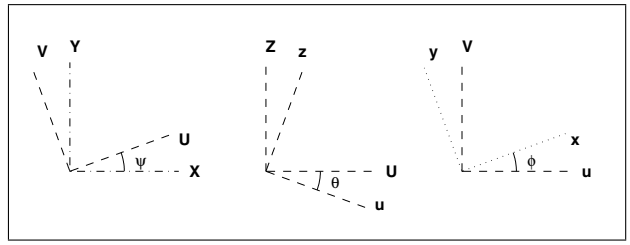

Figure 4. Elementary rotations involved in Figure 3.

be driven around a stationary point O where a perfect binding is assumed. In practice, the user's hand is not stationary but the path of the slat is almost circular [7]. Thus the present assumptions are compatible with the experimental evidence as long as the displacement of the hand remains much smaller than the radius of the circular path. The motion is described in a stationary frame of reference $\mathcal{R}_0 = (O, \mathbf{X}, \mathbf{Y}, \mathbf{Z})$, $\mathbf{Z}$ being the principal axis of rotation (whirl axis).

The string is assimilated to a straight line of constant length along the main axis of the slat, L being the distance OG to the center of gravity of the slat and l its length. The whole bullroarer is seen as a rigid solid with no deformation except the string twist. The mass of the string and the gravitational forces are neglected as not of primary importance. Furthermore, the weak shortening of the string resulting from the twist is also neglected.

The slat position in the fixed frame of reference is defined by the angles (ψ, θ, ϕ), according to the sketch of Figure 3 and the elementary rotations of Figure 4. The whirl is imposed here in the counter-clockwise direction. Another frame of reference, $\mathcal{R} = (G, \mathbf{x}, \mathbf{y}, \mathbf{z})$, is attached to the slat. ψ, θ and ϕ respectively denote the rotations around the axes $\mathbf{Z}$, $\mathbf{V}$, $\mathbf{z}$.

The first mechanical equation relates the sum of the forces on the slat to the acceleration γ of its center of gravity G as

$$-T\mathbf{z} + \mathbf{F} = M\gamma, \tag{1}$$

where M is the total mass of the slat, assumed to be made of a homogeneous material, T is the string tension and $\mathbf{F}$

is the total instantaneous aerodynamic force, supposed to act at point G. For convenience, $\mathbf{F}$ is defined by its components (F_u, F_V) in the frame $(\mathbf{u}, \mathbf{V})$. It has no component along $\mathbf{z}$.

Equation (1) is better expressed in the intermediate frame of unit vectors $(\mathbf{u}, \mathbf{V}, \mathbf{z})$ (Figure 4). A constant whirl is imposed here, so that one can set $\ddot{\psi} = 0$ and $\dot{\psi} = \Omega$, which is a reasonable simplification with respect to the use of a bullroarer. In practice, the driving frequency is varied by the user to change the sound pitch, but this refinement is ignored as not essential for the physical understanding. The following set of scalar equations is obtained:

$$\frac{F_u}{ML} = \ddot{\theta} - \Omega_0^2 \sin\theta\cos\theta, \tag{2}$$

$$\frac{F_V}{ML} = 2\Omega_0\dot{\theta}\cos\theta, \tag{3}$$

$$-\frac{T}{ML} = \dot{\theta}^2 + \Omega_0^2 \sin^2\theta. \tag{4}$$

F_u and F_V are related to the instantaneous lift and drag forces F_L and F_D respectively defined normal to and along the equivalent lateral flow on the slat, by the relations:

$$F_u = F_L \sin\alpha - F_D \cos\alpha,$$
$$F_V = -F_L \cos\alpha - F_D \sin\alpha,$$
$$\text{where} \quad \tan\alpha = \frac{\dot{\psi}\sin\theta}{\dot{\theta}}.$$

Simply stating the running of the bullroarer, the main effect of T is to balance both the centrifugal force and the lift force due to the Magnus effect, whereas the drag force is automatically balanced by imposing a constant whirl.

Applying next the theorem of moments yields:

$$\left(\frac{\mathrm{d}\mu_G}{\mathrm{d}t}\right)_{\mathcal{R}_0} = \mathbf{M} - S\mathbf{z}$$

where $\mu_\mathbf{G}$ is the kinetic moment. $\mathbf{M}$ is the aerodynamic moment vector, essentially along $\mathbf{z}$, and S a return torque due to the string twist, both functions of time or angle ϕ. Even if projected in the frame $(G, \mathbf{u}, \mathbf{V}, \mathbf{z})$, the moment equation leads to quite complicated scalar equations. For the sake of our application, only the projection along $\mathbf{z}$ is retained. With the same hypothesis of constant driving as in the force equation, it reads

$$(A-B)\left[\Omega_0\dot{\theta}\sin\theta\cos 2\phi + \left(\Omega_0^2\sin^2\theta - \dot{\theta}^2\right)\frac{\sin 2\phi}{2}\right] + C\left(\ddot{\phi} - \Omega_0\dot{\theta}\sin\theta\right) = M_z - S. \tag{5}$$

In equation (5), M_z is the projected component of $\mathbf{M}$. A, B and C are the moments of inertia around the axes $\mathbf{x}$, $\mathbf{y}$ and $\mathbf{z}$ respectively, elements of the diagonal matrix of inertia in $\mathcal{R}$. As source terms, M_z and S are assumed known functions of ϕ. As far as the natural motion of a bullroarer is considered, no additional braking torque occurs due to mechanical frictions. Such frictions would arise, however, were the spinning body equiped with ball bearings, which is the case in some of the experiments referred to or described later on in the paper. This effect could be accounted for by simply adding another function of $\dot{\phi}$ to the right-hand side of equation (5).

The set of mechanical equations (2) to (5) can be solved by standard finite differences in time, provided that the source terms F_L, F_D, M_z and S are known. In the present paper, the return torque from the string S has been measured for several kinds of simple or double strings under various tensions (see section 5). The aerodynamic forces and moment F_L, F_D, M_z are *a priori* much a difficult input data to provide, since they require unsteady computational fluid dynamics (CFD).

Strictly speaking, both the slat mechanical equations and the Navier-Stokes equations are coupled in the present case. The instantaneous spinning rate is a solution of the full equations of motion through $\dot{\phi}$, and $\dot{\phi}, \dot{\theta}$ determine the current values of the aerodynamic forces and moment. In the same time, the latter enter the mechanical equations as source terms. Solving the full problem exactly would be a hardly manageable task. A decoupling is better considered here, based on the following arguments. $\dot{\phi}$ only changes slowly in time with regard to its characteristic periods, this being precisely the origin of the psychoacoustic features outlined in section 1. Thus, during a spinning period, the aerodynamic forces and moment $(\mathbf{F}, M_z)$ can be inferred from the equivalent two-dimensional problem of a thin airfoil with elliptic cross-section spinning at constant rate $\dot{\phi}$ in a uniform flow. This problem is solved numerically, only for a reasonably limited set of discrete values of $\dot{\phi}$. Then the amplitude variations of $(\mathbf{F}, \mathbf{M_z})$ are synthetized as continuous functions of $\dot{\phi}$, by interpolating the results by simple closed form expressions. The heavy computational step is made independently, only once. The aerodynamic forcing terms are adjusted at each time-step from the fast-running interpolation and introduced at the next time-step in the mechanical equations.

3.2. Acoustical Equations

The aerodynamic sound generated by the slat is deduced here from the acoustic analogy of Ffowcs Williams and Hawkings [5, 9]. Only a minimum mention of the analogy is given as a theoretical background. Further details can be found in the referenced papers. According to the analogy, the disturbed flows induced by a moving body and the body itself can be replaced by equivalent acoustic sources in motion, radiating as if the surrounding fluid were unbounded and perfectly at rest. For a finite body of surface S in free space and assumed rigid, the acoustic pressure at a point $\mathbf{x}^o$ in the far field, in the sense that the distance is large with respect to a characteristic acoustic wavelength, is then given by [9]:

$$p'(\mathbf{x^o}, \mathbf{t}) = \frac{1}{4\pi}\int_{\mathcal{V}_e}\left[\frac{R_i R_j}{c_0^2 R^3(1-M_r)} \cdot \frac{\partial}{\partial t'}\left(\frac{1}{1-M_r}\frac{\partial}{\partial t'}\left(\frac{T_{ij}}{1-M_r}\right)\right)\right]\mathrm{d}\vec{y} + \frac{1}{4\pi}\int_S\left[\frac{R_i}{c_0 R^2(1-M_r)}\frac{\partial}{\partial t'}\left(\frac{P_i}{1-M_r}\right)\right]\mathrm{d}S_y$$

$$+\frac{1}{4\pi}\int_{\mathcal{V}_i}\left[\frac{R_i}{c_0R^2(1-M_r)}\frac{\partial}{\partial t'}\left(\frac{\rho_0\Gamma_i}{1-M_r}\right)\right]\mathrm{d}\vec{y}$$
$$+\frac{1}{4\pi}\int_{\mathcal{V}_i}\left[\frac{R_iR_j}{c_0^2R^3(1-M_r)}\right. \tag{6}$$
$$\left.\cdot\frac{\partial}{\partial t'}\left(\frac{1}{1-M_r}\frac{\partial}{\partial t'}\left(\frac{\rho_0V_iV_j}{1-M_r}\right)\right)\right]\mathrm{d}\vec{y}.$$

In this expression, T_{ij} is a generalized stress tensor involving the flow velocity in the outer volume $\mathcal{V}_e$, outside the body (see Lighthill [10] for the exact definition and a discussion), $\mathbf{V}$ and $\mathbf{\Gamma}$ are the velocity field and the acceleration of material points of the body, distributed in the inner volume $\mathcal{V}_i$, $\mathbf{P}$ is the local net force per unit area imposed by the body on the surrounding fluid. $\mathbf{R}$ is the distance vector and $R = |\mathbf{R}|$. M_r is the Mach number of a source point in the direction of the observer and $(1-M_r)$ the Doppler factor. The operator [.] stands for an evaluation of a quantity at the retarded time, e.g. the particular value of the source time $t' = t_e(t)$ when the source at point $\mathbf{y}$ emits the sound which will reach the observer at point $\mathbf{x}^o$ at time t. All integrals are written in a system of coordinates attached to the moving body.

The terms in the right-hand side of equation (6) with double derivatives are called quadrupoles, whereas the other two are called dipoles. It is well justified by dimensional analysis [9] that quadrupoles are efficient sources only at higher Mach numbers. In the case of the bullroarer, where the Mach number is very small, typically about 0.03, they can be neglected. Furthermore, again for low Mach numbers and especially for a flat body in strongly unsteady aerodynamic conditions, the acceleration dipole $\mathbf{\Gamma}$ is negligible when compared to the force dipole $\mathbf{P}$. As a consequence, the second source term in equation (6) is definitely dominant. This term is called loading noise.

Now the surface integral means that the elementary sounds coming from every point in the source domain must be summed accounting for differences in emission time. If these differences remain small when compared to a typical period of the sound radiated, they can be neglected and the source domain is said to be compact. In such conditions, the integration and the evaluation at the retarded time commute in the equation. Stated in other words, a sufficient condition for compactness is: $\ell/(1-M_r) \ll \lambda$, $\lambda = c_0T_s$ being the acoustic wavelength and ℓ the size of the body. For the slat of a bullroarer a typical frequency is 100 Hz and a typical length is 30 cm, so the slat is acoustically compact and can be assimilated to a single moving source at point G. Thus equation (6) reduces to the formula first derived by Lowson [11]:

$$p'(\mathbf{x^o},\mathbf{t}) = \frac{-1}{4\pi}\left[\frac{R_i}{c_0R^2(1-M_r)^2}\right.$$
$$\left.\cdot\left(\frac{\partial F_i}{\partial t'}+\frac{F_i}{1-M_r}\frac{\partial M_r}{\partial t'}\right)\right], \tag{7}$$

where $\mathbf{F}$ is the instantaneous aerodynamic force imposed on the slat by the fluid, including lift and drag, integrated over the surface. Furthermore, since M_r is small and the driving frequency is very small when compared to the fundamental source frequency ($T_0 \ll T_s$), the term accounting for the acceleration of the slat can again be reasonably dropped in equation (7), simply giving:

$$p'(\mathbf{x}^o,t) \simeq \frac{-1}{4\pi}\left[\frac{R_i}{c_0R^2(1-M_r)^2}\frac{\partial F_i}{\partial t'}\right] \tag{8}$$

Equation (8) states that the sound radiated by a bullroarer is essentially produced by the fluctuations of the aerodynamic forces on the slat but not by the mean values of these forces. For simplicity, the aerodynamic forces are assumed independent of the spanwise coordinate in this paper; this is quite a good approximation if l/L is small enough. These forces will be considered as known functions of the emission time, deduced from the computations of section 4. Equation (8) also suggests that the retarded-time equation, relating the reception time t and the corresponding emission time $t' = t_e(t)$, must be solved as a necessary preliminary step before calculating the acoustic signal from the kinematics and the aerodynamics of the slat. This equation reads $t_e = t - R(t_e)/c_0$. Since it is an implicit equation for moving sources, this part of the calculations is cumbersome. A much more efficient procedure is to use what is called the 'advanced time' approach [12], applied in the present paper as follows. The source time t' is the one used as the discretized time variable when solving the equations of motion of section 3.2. Its emission value t_e is related to the reception time t by the explicit equation $t = t_e + R(t_e)/c_0$, so that the reception time can be considered as a simple additional variable produced by the solving procedure. Regularly spaced emission time steps correspond to unevenly spaced reception times, but this is not a drawback for a low Mach number motion, since the unevenness is not sufficient to imply a significant undersampling. The acoustic pressure time history $p'(\mathbf{x}^o,t)$ can be reproduced as well from the set of its values at reception times, by simple interpolation.

It is to be borne in mind that the multipole structure of the acoustic sources in the acoustic analogy is a key point for the basic understanding of the directivity of the bullroarer. As equivalent acoustic dipoles, the source terms F_L, F_D radiate no sound along the axis $\mathbf{z}$ and the radiation efficiency is at its maximum in directions normal to this axis. This will explain some of the modulations observed in Figure 17 and already noticeable in Figure 2. However, as an averaged result of the combined whirling and spinning motions, the bullroarer radiates sound with the same order of magnitude in all directions. This has been confirmed experimentally by Fletcher *et al* [7].

4. Spinning motion and Autorotation Regime

4.1. Preliminaries

The running of a bullroarer obviously shows that sound is generated as the slat spins around its main axis $\mathbf{z}$. In

order to better understand this basic mechanism, the two-dimensional problem of a flat elliptic cross-section spinning in a uniform flow is investigated in this section. Around a given instant of time, the slat passing through the air indeed behaves fundamentally like a thin airfoil spinning in a parallel stream, the slat edges being assimilated successively to trailing and leading edges.

The main aerodynamic effect of spinning is that the instantaneous forces on the slat have nothing to deal with what they would be for the same slat held motionless with the current angle of attack with respect to the oncoming flow. Any variation of angle of attack results in shed vorticity, the latter being evacuated in the flow, so that a time delay occurs between this variation and the corresponding variation of the aerodynamic forces. In principle, the problem is stated in the same way as that of an oscillatory airfoil or an airfoil in a gusty atmosphere, usually referred to when studying the unsteady aerodynamics of blades. The difference is that instead of experiencing small variations of angle of attack, the slat continuously rotates. As a consequence, existing linearized unsteady aerodynamic theories do not apply here. The unsteady flow associated with the spinning motion and the precise features of the shed vorticity can only be described by accurate numerical techniques.

In fact, the case of the spinning slat is a specific example of periodic flow, different from both the continuous vortex shedding due to the Kutta condition in the wake of an oscillatory airfoil and the classical von Kármán vortex street behind bluff bodies, as depicted for instance in [9].

The unsteady flow depends on the velocity ratio:

$$\xi = \frac{\Omega c}{2U_0},$$

where $\Omega c/2$ is the tangential velocity of the edges of the slat and U_0 the velocity of the oncoming flow. $\xi = 1$ is equivalent to a condition of rolling contact with no slip of the retreating edge with respect to the undisturbed flow. ξ is the main parameter of the study.

It is to be noted that the computed results presented in the next section are based on the assumption of constant spinning rate, or constant ξ, in a parallel stream, which is not always relevant in practice. They are believed reliable for slats with large inertia and for small ratios l/L. Moreover, they must be used step by step, the true motion of the bullroarer with accelerating or decelerating spinning rate being assimilated to a succession of constant-spinning states.

4.2. Numerical Computations

The numerical analysis was carried out using PROUST, a CFD Reynolds-Averaged, Navier-Stokes code developed by Aubert *et al.* [13, 14]. It has previously been validated and shown to accurately simulate steady and unsteady, inviscid and viscous flows. The code is used as a way to provide the aerodynamic input data necessary for noise computations but the study is not dedicated to the code itself. So only a short description of the numerical approach is given. Specialists will find the main points below and more details in [13, 14]. The space discretization is based on a finite volume formulation with moving meshes, which utilizes vertex variable storage. The convective fluxes are evaluated using Roe's Approximate Riemann Solver. The viscous terms are computed by a second-order centered scheme. Only the unsteadiness induced by the spinning motion is explicitely simulated and the effects of the small-scale turbulence are accounted for by a k-omega model, known to correctly reproduce the separated flow regions.

Compatibility relations are used to take the physical boundary conditions into account. The outgoing characteristics are retained, since these provide information from inside the computational domain. The incoming characteristics, on the other hand, are replaced by physical boundary conditions, i.e. total temperature and velocity components for a very low Mach number subsonic inlet, static pressure for a subsonic outlet, zero velocity and heat flux for an adiabatic wall. Non reflective boundary conditions are implemented by retaining the equations associated to the incoming characteristics, in which the wave velocity is fixed to zero to prohibit propagation directed into the computational domain. The resulting semi-discrete scheme is integrated in time using an explicit five-steps Runge-Kutta time marching algorithm. For current calculations with Mach numbers below 0.08, a CFL number about 0.1 was used (see reference [15] for definitions).

In the present application, the computational domain simulates the two-dimensional flow around an elliptic cross-section of the slat with relative thickness 6.7%. It extends far around the walls up to five chord lengths and rotates as a solid body with the constant speed corresponding to the imposed value of ξ. The mesh used is a structured O-grid, with 201×61 nodes. To enhance the accuracy in the large-gradient zones near the leading/trailing edges and in the boundary layers, the grid density has been significantly increased in those areas. The air is modeled as a viscous perfect gas. The inlet conditions are such that the total temperature is 276.6 K, the velocity, U_0, equals $10.0\,m.s^{-1}$, the turbulence intensity is 4 % and the turbulent-to-laminar viscosity ratio equals 5.0. The outlet static pressure was adjusted to 102.38 kPa.

Examples of computed instantaneous flow patterns are shown in Figures 5 and 6 in terms of turbulent kinetic energy contours, for two different values of ξ. The fluid flows from the left to the right and the slat spins in the counterclockwise direction. The kinetic energy map points at the locii of maximum shear and turbulence production. It is a way to visualize the dominant flow patterns. A well-defined vortex is clearly identified just at the retreating edge, at the bottom of each sub-plot, whereas the upper advancing edge only generates a free shear layer.

The vortex remains attached close to the retreating edge until the slat is almost parallel to the mean flow. Then it is shed and convected away from the slat, interacting with the aforementioned shear layer. The vortex growth is limited to about a quarter rotation cycle. The vortical patterns of Figure 5 are in excellent agreement with experimental

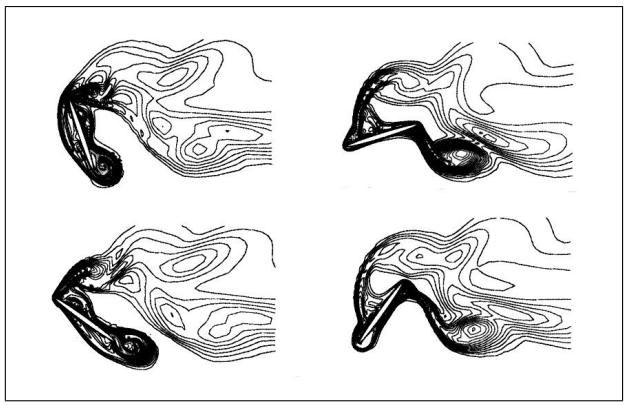

Figure 5. Turbulent kinetic energy contour plots at various time steps in the wake of the spinning slat, $\xi = 0.57$. Flow from left to right, spinning in the counter-clockwise direction.

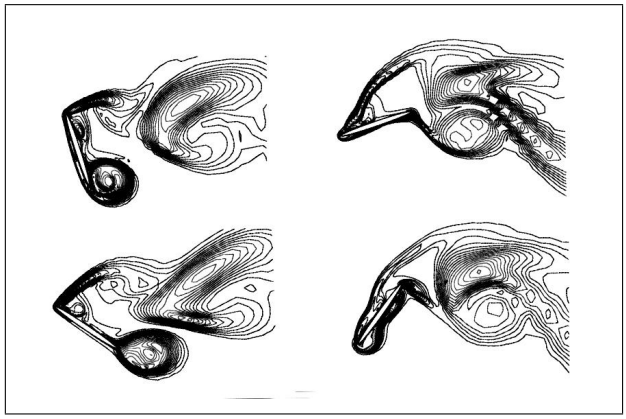

Figure 6. Turbulent kinetic energy contour plots at various time steps in the wake of the spinning body, $\xi = 0.94$. Flow from left to right, spinning in the counter-clockwise direction.

visualizations made around a spinning flat plate at equivalent Reynolds number [16], as reproduced in [17].

The impulsive dynamics of the vortex shed at the retreating edge is typical of the wake behind an autorotating slat. This point is in deep contrast with the well-ordered von Kármán vortex street in the wake of a stationary bluff body, for which the shed vortices dissipate very slowly due to a condition of equilibrium. Furthermore, the single autorotation vortex is formed very near the retreating edge, whereas the von Kármán street generally takes place at a finite downstream distance, with contrarotating vortices. Since the unsteady aerodynamic forces are induced by the circulation of the vortices, some compensation occurs in the vortex shedding behind the bluff body, which does not occur with the bullroarer. So it is not surprising that the bullroarer is a much more efficient sound generator than a stationary bluff body.

4.3. Post-Processing and Model Results

For the sake of solving the mechanical equations of motion and predicting the radiated sound field, simple analytic expressions for aerodynamic forces and moment, deduced from the preceding two-dimensional CFD results, are enough. More precisely, according to section 3, the full aerodynamic moment and forces are needed as input data in the mechanical equations, whereas the time variations of the lift and drag forces are needed for acoustic calculations. The computed quantities have been first post-processed and simplified curves fitted on, ignoring the smallest details in the time signatures. For that fit, only the Fourier coefficients corresponding to the first even harmonics of the fundamental spinning frequency $2f_0$ and $4f_0$ have been retained.

Secondly, the results have been made non-dimensional by introducing characteristic scales in the usual way, in order to provide general expressions. The latter are given here for a flat elliptic cross-section. Their validity should be checked for other slat shapes but the non-dimensional results are believed not to vary to a large extent.

The unsteady drag force F_D parallel to the oncoming flow and lift force F_D normal to the flow are made non-dimensional by introducing the drag and lift coefficients per unit span, defined as:

$$C_D = \frac{F_D}{c(\rho_0 U_0^2/2)}, \qquad C_L = \frac{F_L}{c(\rho_0 U_0^2/2)}. \tag{9}$$

In the same way, the aerodynamic moment coefficient is defined as

$$C_M = \frac{M_z}{\frac{1}{2}\rho_0 U_0^2 c^2}$$

The computed coefficients C_L, C_D and C_M are respectively plotted with symbols in Figures 7, 8 and 9 for the four investigated values of ξ, as functions of the spinning angle ϕ proportional to the relative time t'/T_s. As expected, they have a nearly-sinusoidal behaviour at twice the spinning frequency, except for the smallest value of ξ. A careful inspection of the results shows that the extrema do not reproduce exactly from one semi-revolution of the slat to the next one, indicating subharmonic behaviour at the spinning frequency. The approximations are also plotted in solid lines. The discrepancies do not exceed a few percents and are acceptable for the intended application. They are more pronounced in Figure 9, which is attributed to the enhancement of numerical errors in the extraction procedure of M_z from the computed aerodynamic forces.

In a second step, moduli and phases of the smoothed Fourier components have been interpolated by simple functions of the velocity parameter ξ. The averaged values are plotted in Figure 10 and the Fourier coefficients in Figure 11. They are analyzed below separately.

4.3.1. Averaged coefficients

The averaged coefficients deduced from the results of Figures 7, 8, 9 are indicated by the symbols in the plots of Figure 10. In principle, the values of the mean drag $\overline{F}_D$ as a function of ξ are extrapolated at best for vanishing ξ to the drag of a slat held normal to the flow, according to the stable position of equilibrium observed in the experiments (see section 5 below). The drag coefficient of an elliptical

ACTA ACUSTICA UNITED WITH ACUSTICA
Vol. 92 (2006)

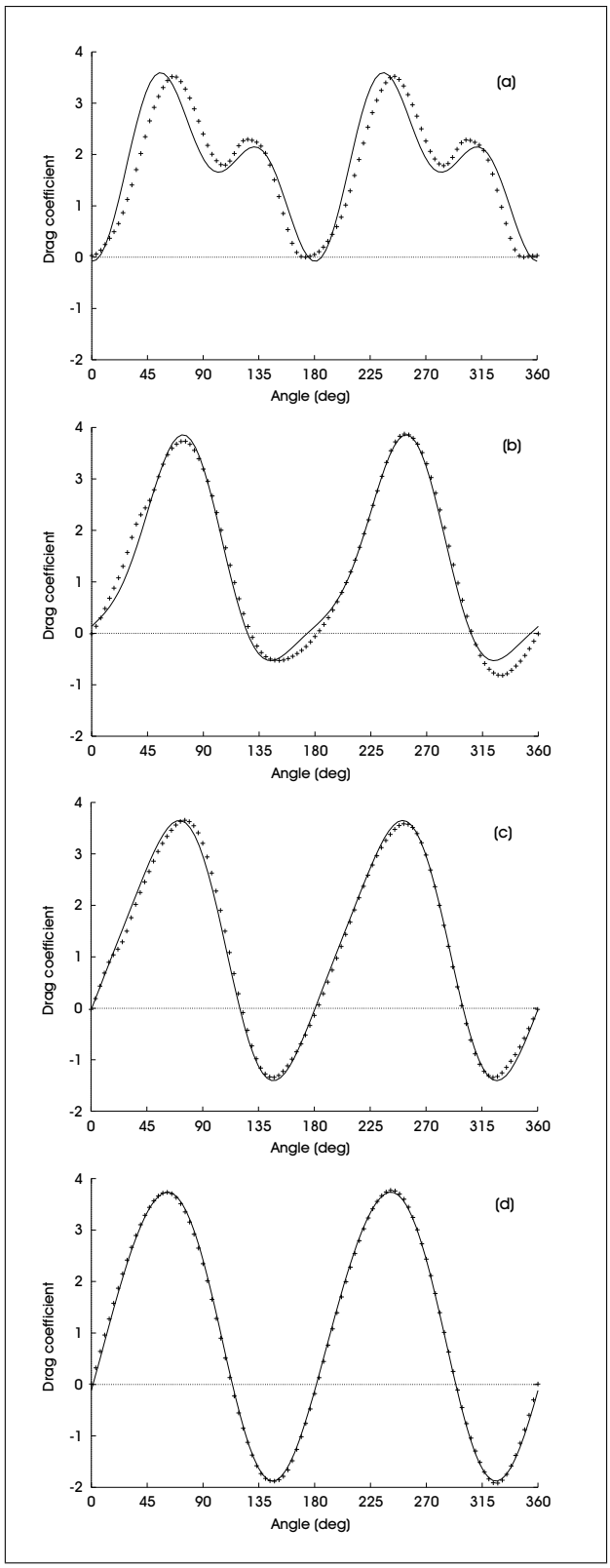

Figure 7. Unsteady drag coefficient. a): ξ=0.19, b): ξ=0.57, c): ξ=0.94, d): ξ=1.50.

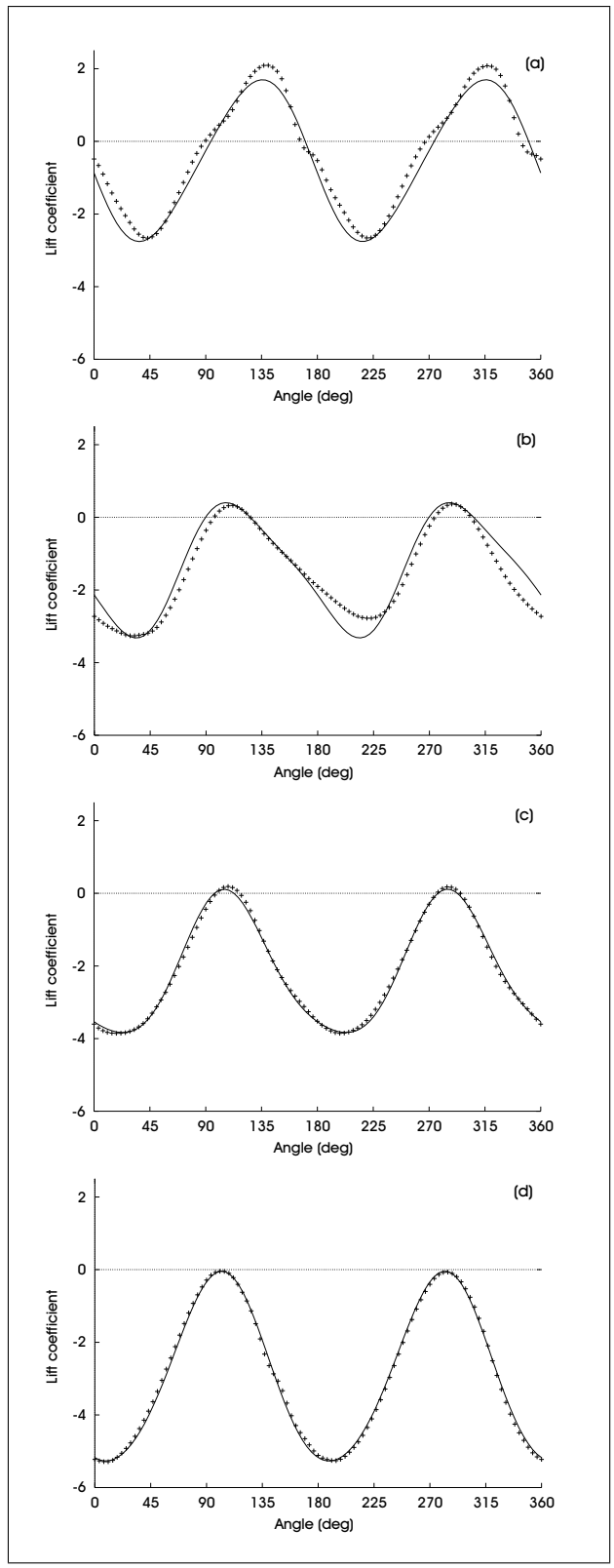

Figure 8. Unsteady lift coefficient. a): ξ=0.19, b): ξ=0.57, c): ξ=0.94, d): ξ=1.5.

cross-section with small relative thickness e/c (e being the maximum thickness and c the chord length) held normal to the flow is about $\overline{C}_{D_0} = 1.9$ [18].

The present computed results suggest a slightly higher value, remaining in quite a close agreement, and are best fitted by the approximate formula:

$$\overline{C}_D = 1 + 1.17\mathrm{e}^{-2.1\xi}. \qquad (10)$$

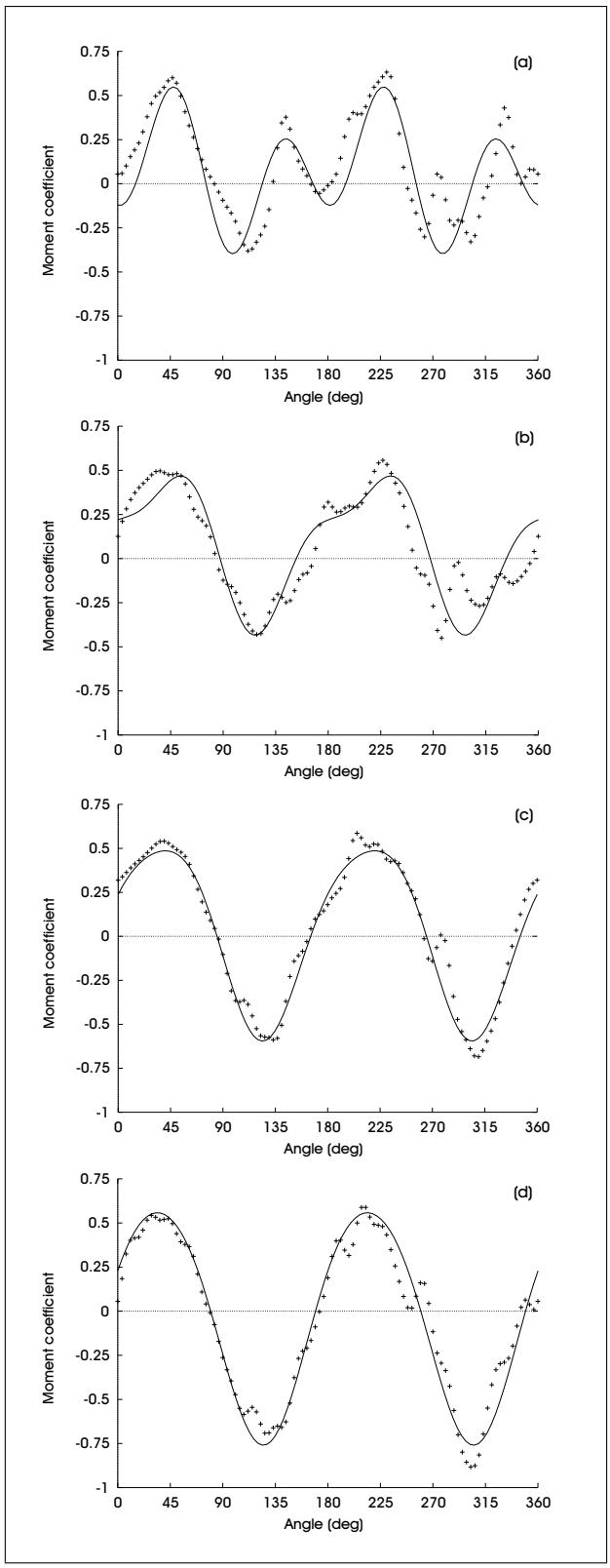

Figure 9. Unsteady moment coefficient. a): ξ=0.19, b): ξ=0.57, c): ξ=0.94, d): ξ=1.5.

The main conclusion is that the spinning progressively reduces the mean drag as the velocity ratio increases.

As expected, it is found that the mean lift corresponding to the Magnus effect is a function of ξ increasing

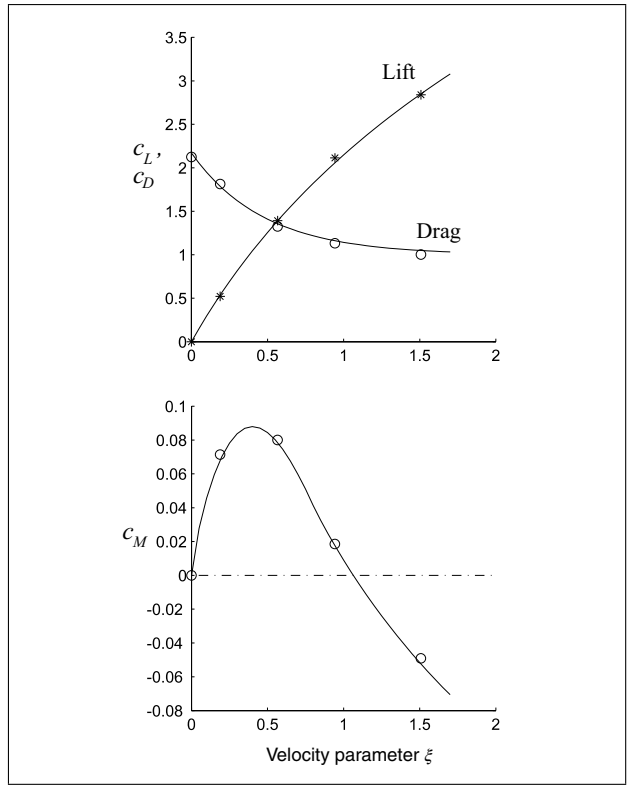

Figure 10. Model variations of the averaged aerodynamic coefficients with the velocity parameter ξ. The symbols denote the present computations and the lines the interpolations.

from zero. The mean lift coefficient lies between 0.4 and 3 within the range covered by the computations. These values are significantly higher than those for a cylinder with circular cross-section of diameter equal to c at the same Reynolds number and spinning with the same velocity parameter (Comolet [19]). The difference may be attributed to the strong imbalance induced by the single vortex at the retreating edge, that has no counterpart from the opposite edge. Furthermore, the negative values of $\overline{C}_L$ for a cylinder at lower values of ξ, attributed to boundary layer separation, are not observed here.

The computed results are best fitted with the following formula:

$$\overline{C}_L = 3.1 \ln(1 + \xi). \tag{11}$$

Finally, the average value $\overline{C}_M$ of the aerodynamic moment is completed by the necessary condition of zero moment at zero velocity ratio. The moment is again zero for $\xi \simeq 1$, corresponding to the state of autorotation. It is positive (accelerating) for ξ <1 and negative (decelerating) for ξ >1. The results can be interpolated as

$$\begin{aligned} \overline{C}_M &= 0.088 \sin(\pi \xi^{0.76}), && 0 < \xi < 0.8, \\ \overline{C}_M &= 0.088 \sin(\pi (0.8)^{0.76}) && \\ &\quad - 0.196(\xi - 0.8) + 0.075(\xi - 0.8)^{1.5}, && \xi > 0.8. \end{aligned} \tag{12}$$

This suggests that the spinning motion of a slat suddenly disturbed from its stable equilibrium *a priori* accelerates

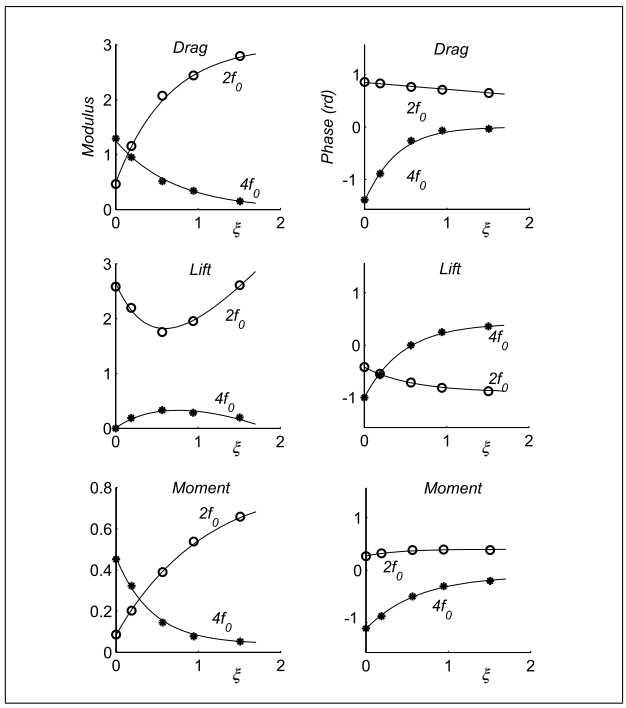

Figure 11. Model variations of the moduli and phases of the aerodynamic coefficients with the velocity parameter ξ. The symbols denote the present computations and the lines the interpolations. Fourier components at $2f_0$ ($\circ$) and $4f_0$ ($*$).

from rest as long as $\xi < 1$, till it reaches the autorotation state. Situations with $\xi > 1$ should not be encountered, since they correspond to aerodynamic braking, except at the beginning of a semi-cycle of inversion of a bullroarer because of inertia. It is to be noted that the negative $\overline{C}_M$ pointed out by Lugt [20] for very small values of ξ in a similar study on the basis of a vortex method was not observed in the present computations. This difference has not been further investigated. It has no effect in the present application, precisely because in the case of the bullroarer, the return torque from the string is maximum when ξ is zero and dominates the mechanical behaviour around reversals.

4.3.2. Unsteady coefficients

Though not detailed here, similar interpolation formulae have been deduced for the amplitudes and phases of the first two Fourier components of the aerodynamic coefficients. They are indicated by the solid lines of Figure 11 for frequencies $2f_0$ and $4f_0$. The phase information is recognized as very determinant, both for the acoustic signature as well as for the general kinematics of the bullroarer. Autorotation is self-sustained due to a proper phase-shift between the aerodynamic moment M_z and the moment of inertia of the slat around the **z** axis. Up to that point, it follows from the computed or interpolated results that the phases of all quantities vary continuously with ξ, when referred to angle ϕ. Furthermore F_L and F_D oscillate almost in phase quadrature at $2f_0$.

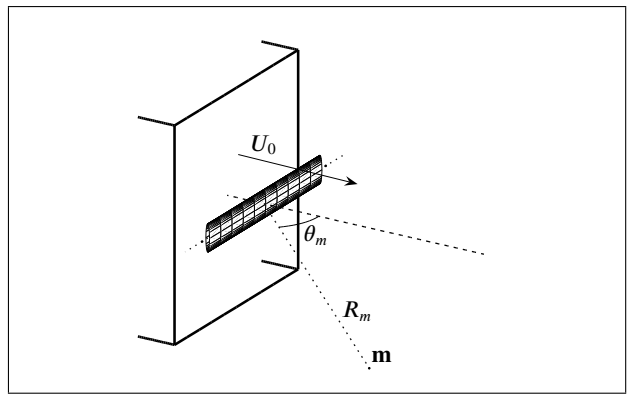

Figure 12. Coordinates in the experimental set-up for the study of autorotation noise. θ_m is the direction of the observer with respect to the oncoming flow.

5. Experimental Study

5.1. Experimental Set-Up and Initial Conditions

Extensive computations and experiments about the autorotation of a flat plate or a symmetric two-dimensional airfoil with elliptical cross-section are reported in the literature (Lugt *et al.* [21], Iversen [17], Lugt [20, 22]). The main objective here is not to deeply investigate autorotation again, since previous studies cover the matter with systematic attention, but rather to characterize autorotation from the aeroacoustical point of view. This point, to the authors' knowledge, is not treated elsewhere, in the sense that the work reported by Fletcher *et al* [7] does not address the connections with the autorotation phenomenon and the general background of the acoustic analogy. By the way, the experiments help to place the present contribution within the range of the works by previous investigators. Furthermore, the experimental results are used to validate the simulation program.

Measurements were carried out in a small anechoic chamber with open-jet wind tunnel. The model rectangular slat used in the experiment has the same elliptical cross-section as in the computations. Thickness and span are 4 mm and 280 mm respectively, the chord length being 60 mm. The model is completed by an axis inserted in the inner ring of small-size ball bearings. The outer ring of the bearings is held rigidly to the nozzle of the wind tunnel, according to the sketch of Figure 12. The nozzle dimensions are 300 mm by 300 mm. The range of parameters is close to the one investigated by Fletcher *et al.* [7].

Though the maximum achievable flow velocity U_0 is 20 m/s, autorotation has been only investigated below 13 m/s, in order to avoid mechanical dammage and especially distortions in the results because of the deformation of the model-and-axis arrangement due to the mean drag. These drawbacks are not serious, since the range of parameters corresponding to typical bullroarer applications is covered. This leads to the limit value $5 \cdot 10^4$ of the Reynolds number based on the slat chord length. Both deformations and natural frictions inside the bearings are responsible for an unavoidable braking torque. As pointed

out by Iversen [17], the braking torque artificially reduces the value of $\xi = \Omega c/(2U_0)$ at autorotation, with respect to what it should be in the conditions of free spinning. The model axis has been fixed close to the nozzle lips, in order to minimize interactions with the turbulent shear layers of the wind tunnel flow. It was assumed implicitely that the presence of the nozzle itself has no significant effect on the autorotation process and a negligible scattering effect on the acoustic radiation at angles θ_m to the flow less than 90 degrees.

A Bruel&Kjaer 1/2' microphone was mounted on a rotating support (at point **m** of Figure 12), providing acoustic measurements in a horizontal plane normal to the mid-span plane and including the model axis, at a distance $R_m = 1.3$ m from the slat center of gravity. This is believed to ensure a satisfactory condition of acoustic far-field in the sense that $2\pi R_m$ is larger than the characteristic wavelength, as well as geometric far-field in the sense that R_m is much larger than the slat span l. The cut-off frequency of the anechoic room is around 80 Hz, slightly higher than the fundamental autorotation frequency. It is expected to have no effect on the results, because the amount of reflection on the glass-wool structures remains small, on the one hand, and because the propagation path of the residual wall reflections is larger than the direct sound path.

Increasing flow velocity from zero with the model slat initially at rest does not result in any rotation. The slat quickly orientates with the chord line normal to the oncoming flow. This is the stable position of equilibrium. The other position of equilibrium, with the chord line parallel to the flow, is obviously unstable. As the flow is on, a given initial impulse is necessary to force the slat to spin but, as soon as initialized, the spinning accelerates rapidly, reaching the autorotation state. Autorotation is self-sustained. As the oncoming flow velocity U_0 is further varied, the spinning rate changes automatically, increasing with increased U_0.

Similar features are commonly observed in nature with regard to falling leaves or seeds. In the same way, for instance, a visit card held in a horizontal plane above the ground and suddenly released falls to the ground, remaining parallel to it and following a vertical path. If initially held normal to the ground (in a vertical plane), the card begins to spin around its larger axis and, instead of falling vertically, is deviated along a curved path by the Magnus effect.

These observations help to understand the behaviour of a bullroarer as follows. A weak initial rotation of the slat around its main axis, achievable by back-and-forth balancing of the string or small impact on the ground, for instance, is necessary to ensure the proper rotation when starting to whirl the bullroarer through the air at angular speed Ω_0. Sometimes, the stable position of equilibrium is preserved, with no rotation around the $\vec{z}$ axis, and no noticeable sound is heard, except a very weak gentle hiss attributed to the vortex shedding in the string wake.

If correctly started, Ω_0 being constant, the spinning motion accelerates until it reaches the free autorotation condition, provided that the string return torque is reasonable. This torque progressively increases as the string is twisted, so that it finally brakes autorotation. The braking and return torque are strong enough to make the spinning drop and restart in the opposite sense for a new autorotation half-cycle.

As long as the stable position of equilibrium is maintained in the wind-tunnel experiment, no noticeable sound is measured around the slat, despite the natural von Kármán vortex shedding, the expected frequency of which is between 50 and 100 Hz. In contrast, the vortex shedding behind a bluff body or a circular cylinder of same wetted front surface would be audible. The usual von Kármán vortex street is known to induce relatively large fluctuations normal to the oncoming flow and much weaker fluctuations parallel to that flow [23]. Since the slat cross-section remains normal to the flow in the equilibrium state, the induced pressure fluctuations normal to the flow are distributed over a very small surface and the much weaker streamwise ones over a larger surface: the net integrated forces must be very small, providing negligible acoustic sources.

5.2. Results

The results of this section are expressed in terms of decibels, using either the pressure level SPL_{dB} or the intensity level IL_{dB}, defined as:

$$\mathrm{SPL}_{dB} = 20\log_{10}\left(\frac{\sqrt{\langle p'^2\rangle}}{2\cdot 10^{-5}}\right),$$

$$\mathrm{IL}_{dB} = 10\log_{10}\left(\frac{(\langle p'^2\rangle/(\rho_0 c_0)}{10^{-12}}\right),$$

and equivalent in the far field.

A typical sound is generated during autorotation, the pitch and level of which are increasing functions of flow velocity. The main features of this sound as measured on the wind tunnel set–up are gathered in Figure 13.

As expected, the acoustic spectrum, Figure 13-a, is almost discrete-frequency in nature. It exhibits sharp peaks at twice the spinning frequency $2f_0$ and harmonics. All the intermediate frequencies $(2n+1)f_0$ appear as well, though with much lower levels, showing that phenomena do not exactly reproduce every half-rotation of the slat. These odd multiples can be ignored to get a first insight, certainly having only a weak effect on the psychoacoustic signature. However, they do make sense. The practical difficulty to ensure a perfect alignment of the axes and to avoid imbalance could be mentioned as an explanation for the occurence of the spinning frequency as the fundamental frequency instead of twice that value. However, the investigations of Iversen [17] show that the rotation speed does vary significantly over one revolution, especially for bodies with small inertia, providing another explanation. Moreover, the same observation was made in section 3 from the computed results, despite the imposed constant spinning rate, suggesting that the subharmonic behaviour

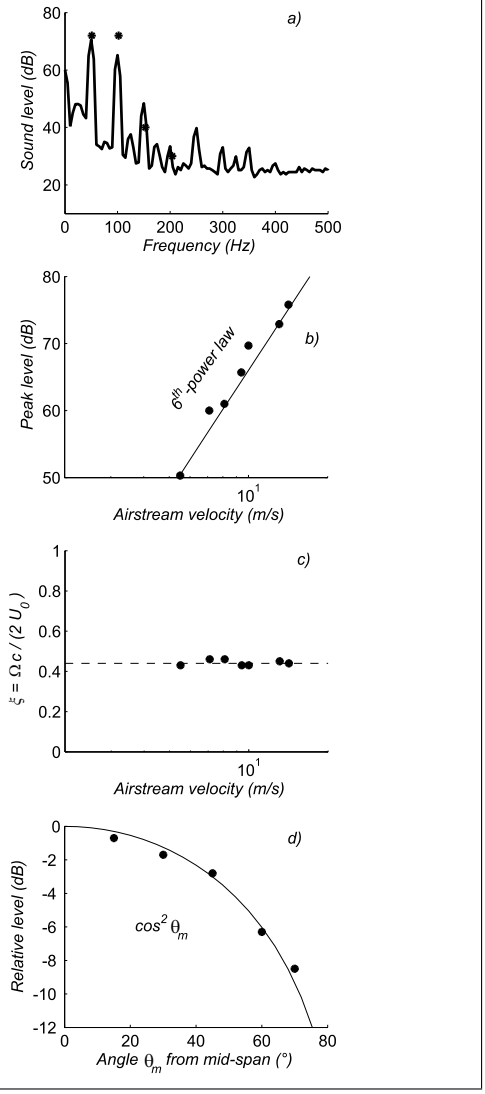

Figure 13. Typical results for autorotation noise of the model slat in wind-tunnel testing. (a): far field spectrum at $1.3m$ from the slat center for $\theta_m = 45°$, $U_0 = 11$ m/s (black dots stand for the computed levels from a subsequent section). (b): 6^{th}-power scaling law of the acoustic intensity, assessed on the level of the fundamental frequency. (c): evidence of a nearly constant spinning rate $\xi(U_0)$. (d): dipolar directivity in the horizontal plane, normal to mid-span.

is also partially due to some non-linearity of the flow inherent to the autorotation mechanism. By the way, it can be guessed that the acoustic signal from a bullroarer of non symmetrical cross-section would exhibit a larger amplitude at the subharmonic frequencies, since different flow patterns would be generated around both edges.

The second plot in Figure 13b shows that the sound intensity at the fundamental frequency increases like the oncoming flow velocity to the sixth power. This is exactly the expected trend for a compact dipole in aeroacoustics, from dimensional analysis arguments. However, the sixth-power law only holds because the spinning frequency remains proportional to the flow velocity, which corresponds to a constant value of ξ in the experiment, as featured in the third plot, Figure 13c. More precisely, from equation (8), the acoustic pressure p' is proportional to the time derivative of the aerodynamic force $\partial F/\partial t'$. Thus assuming a cyclic variation with angular frequency ω makes the pressure proportional to ωF. If ξ is constant, ω must be proportional to U_0 and the modulus F is proportional to U_0^2 from equation (9). As a result, the acoustic intensity scales like U_0^6.

The experimental evidence may depart from this trend if different circumstances are encountered. Once during the experiment, a sudden spinning acceleration has been observed without variation of the flow velocity U_0, attributed to an unexplained drop of the friction and boundary conditions at the ball bearings. A much louder sound was heard, suggesting that the sound level is also an increasing function of the velocity ratio ξ. Unfortunately, the corresponding conditions were impossible to reproduce with the present set-up, which does not allow to vary ξ because of the lack of an external driving device. The louder sound is explained by the increase of ω corresponding to the increase of ξ, on the one hand, and essentially to the resulting larger value of the lift force component at $2f_0$ expected from Figure 11, on the other hand. It is to be noted that, due to the relatively high braking torque in the experiment, autorotation does not take place with the natural value of ξ about 1, but a lower one, about 0.45. Anyway, the consequences of the constant value of ξ during autorotation are twofold. First, the sound pitch of a bullroarer increases linearly with the flow speed. Secondly, for a given flow speed, the sound pitch must be inversely proportional to the chord length. This point, reported elsewhere, has not been fully verified in the present wind-tunnel experiment. It is confirmed by the computational results of section 4.2, which hold in non-dimensional variables.

The last plot in Figure 13d shows measurements performed at different angles θ_m to the flow direction in a horizontal plane containing the slat axis, normal to the mid-span plane. The radiated sound tends towards its maximum in the mid-span plane ($\theta_m = 0$) and decreases like the function $\cos\theta_m$. Note that the measurements cannot be made exactly in the mid-span plane, because the microphone would be inside the flow from the wind tunnel and would measure the aerodynamic pressure associated with the turbulence of the jet mixing with the quiescent air of the anechoic room. Again the observed trend is in accordance with the expected directivity pattern for a compact dipole with axis rotating in the mid-span plane, since from equation (8),

$$\frac{\mathbf{R}}{R}\cdot\frac{\partial\mathbf{F}}{\partial t'} = \cos\theta_m\frac{\partial F}{\partial t'}$$

if F denotes the algebraic value of $\mathbf{F}$.

5.3. Hand-Driven Experiments

Another series of measurements has been performed in the anechoic room with hand-driven bullroarers to highlight the specific acoustic features encountered in practice. The whirling frequency was checked by making the user obey

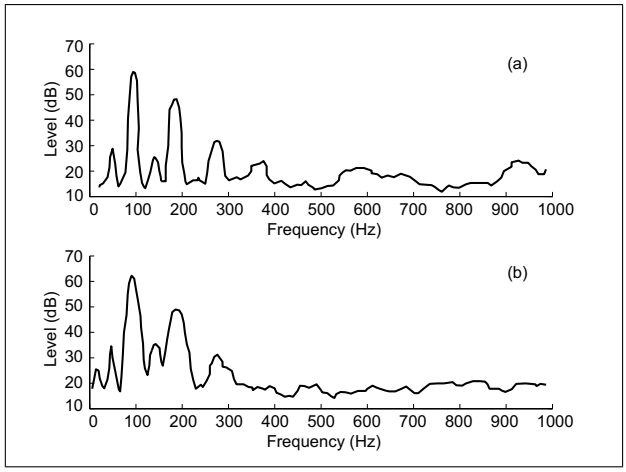

Figure 14. Sound spectra measured on the whirl axis (a) and normal to the axis (b) for a bullroarer with ball bearings in stabilized autorotation.

the clockwork regularity of a metronome, tuned to ensure one or two revolutions per second with a mean radius L equal to 0.8 m. This leads to typical values of the relative speed U_0 on the slat of about 5 to 12 m/s, roughly covered by the wind-tunnel experiment.

A prototype equiped with ball bearings at the junction between the string and the slat has been first tested to ensure a stabilized autorotation in the presence of constant whirl. In that case the slat follows a perfectly circular path and the string remains continuously on the same conical surface. Because the string twist and the corresponding return torque are deactivated, the sound emitted is only modulated by the circular motion. Sample sound spectra for microphone locations exactly at 90° to and on the **Z** axis are plotted in Figure 14a and b. The whirl is fixed at 138 rpm, with a slat chord length $c = 4$ cm. This leads to a tangential relative speed $U_0 = 11.6$ m/s. The fundamental frequency at 95 Hz corresponds to a spinning frequency of 47.5 Hz, thus a velocity ratio $\xi \simeq 0.52$. This is much less than the theoretical value 1 according to pure aerodynamical arguments, and the difference is again attributed to mechanical friction in the ball bearings. Three to four peaks are observed on the figure. Sub-harmonics are clearly noticeable, which confirms that the presumably associated non-linear effects are inherent to the stabilized autorotation, independently of the whirling motion. The peaks are quite sharp when the listener lies exactly on the whirl axis and show additional broadening when the listener is at 90° from the axis, apart from the difficulty for the user to sustain a perfectly periodic whirl. Since the Mach number U_0/c_0 is 0.036 in that case, the spectral broadening due to the Doppler effect makes the fundamental frequency oscillate by an amount of ±3.5 Hz, which is small but noticeable. This explains partially the difference between the plots of Figure 14a and Figure 14b. It is also to be noted that the source-to-microphone distance is constant for an on-axis microphone and varies significantly here for a microphone off the axis, due to the relatively short distance of $4m$ in the anechoic room.

Finally measurements have been made with a true bullroarer, including the full mechanical details and, essentially, the string return torque. The sound was measured again 4 meters from the cone apex of the bullroarer, for the same two configurations: exactly along the **Z** axis ($\theta = 0$) and in the perpendicular plane ($\theta = \pi/2$). A typical time-frequency analysis of the radiated sound has already been given in Figure 2 of section 2 for $\theta = \pi/2$. The results are not essentially modified at other angles and/or other velocities. The main difference is that the secondary wave packets of Figure 2 at the whirling period are well separated whereas they would be much less so for a microphone on the **Z** axis, due to the quasi invariance in time, of the relative location and orientation of the source with respect to the observer.

Indeed, measuring the sound radiated in a direction perpendicular to the **Z** axis makes the distance from the slat to the microphone vary significantly if the far field distance is not much larger than the circular path radius. Another point is the effect of the slat directivity as clearly identified in Figure 13d. This will be addressed later on in section 6.

Some secondary effects, such as surface roughness, serrated edges (see the rectangular bullroarer of Figure 1) and so on, have not been investigated here. Even though mention is made in the literature of an essential effect of a one-sided unevenness [4], this is not found to be necessary at all. Autorotation takes place with a perfectly symmetric slat cross-section, indicating that geometrical details are not determinant and only lead to express faint differences in the fundamental mechanism. Nevertheless, roughness and non-symmetrical cross-section can help to start the spinning motion by inducing some initial imbalance.

5.4. String Return Torque

The return torque S is a necessary input in the physical model. In order to characterize S, a very crude device was used here. The principle is as follows. A single or double string is attached at both ends with no possible rotation. Only one end is allowed to translate parallel to the string direction, so that a constant tension T can be applied by hanging weights. The initial length with no twist is slightly reduced during the experiment, exactly as in the case of a true bullroarer. One end of a small light level arm is attached normal to the string at mid length and progressively wound, inducing inverse twist on each half-string. The free end of the level arm is supported by a letter-balance. The force at this end and the corresponding torque are measured as functions of the string twist in terms of number of revolutions per unit initial length, for different values of the tension T.

A string made of vegetal fibers has been chosen for the experiment. Again the aim was not to fully investigate the problem of string twist, but only to get orders of magnitudes and typical laws of variation.

Sample results are plotted in Figure 15. It is seen that the return torque increases with both tension and twist, but that the variations are not linearly related. The torque of a double string is more than twice the one of a single string, due

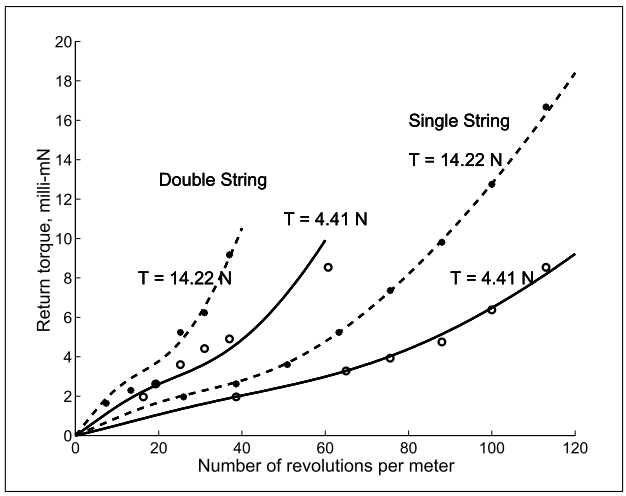

Figure 15. Return torque as a function of twist, for strings made of vegetal fibers.

to frictions and mutual interactions. For the highest values of the twist, the return torque increases as the squared number of revolutions, whereas a moderate twist produces a small torque. More precisely, the initial data are interpolated quite well by the following formula:

$$S = 9.81 \cdot 10^{-5}\left(a\nu^2 + \eta\nu e^{-2.3(\nu/b)^2}\right), \qquad (13)$$

where ν is the number of revolutions per meter of initial length and S is in 10^{-3} mN. η, a and b are functions of T. For respectively the simple (index s) and double (index d) vegetal strings used in the experiments, these are:

$$a_s = 2.18T - 0.3351T^{3/2}, \quad a_d = 8.4T - 0.98T^{3/2},$$
$$b_s = 93e^{-0.0446T}, \quad b_d = 47e^{-0.0446T},$$
$$\eta_s = 230\sqrt{T}, \quad \eta_d = 680\sqrt{T},$$

T being in N.

The present experiment only provides indicative results. Different values could be obtained from other types of strings. However the non-linear increase certainly is a general trend. Furthermore, running the bullroarer with the same string again and again induces progressive changes associated with the string aging, mainly due to the breaking of vegetal fibers, that turn to reduce the return torque at moderate twist. Finally, the return torque appears to be the most difficult parameter to assess properly. What must be retained for the sake of feeding a consistent model is that a moderate twist does not generate noticeable torque, till a specific compromise between the number of revolutions and the tension is achieved; then increasing twist causes a fast torque increase. This helps to understand why the bullroarer sounds almost stabilized during the time intervals of moderate twist.

6. Aeroacoustic Simulation of the Bullroarer

Finally, solving first the mechanical equations of section 2 together with the approximate formulae for the functions F_D, F_L and M_z, and then applying the acoustic equation (8), leads to a complete physical model of the bullroarer. It can be noticed that the bullroarer, unlike usual rotating blade configurations, is a specific aeroacoustic example, in which the source motion is not prescribed but must be determined from a preliminary knowledge of the basic properties of the flow field.

The simulation program has been first tested on the simplified configuration of stabilized autorotation from a simplified form of the equations (2) to (5), corresponding to the absence of whirl and return torque. In that case, as soon as started, the spinning motion tends asymptotically towards the autorotation state, whatever the initial condition is. Though not plotted here, the solution of the mechanical equations exhibits small oscillations around the limit, due to the unsteadiness in the aerodynamic moment; the higher the density of the slat is, the lower they are.

The wind-tunnel experiment of section 5 can be directly simulated from equation (8) without solving the equations (2) to (5), if the CFD results of section 4 are used directly with the measured value of ξ about 0.45. This has been attempted and led to the computed averaged acoustic spectrum of Figure 16, to be compared to the measured spectrum of Figure 13a. A pretty good agreement is found, especially if the measured levels are slightly enhanced to account for the additional spectral spreading in the experiment. The accuracy is within 1 dB at the fundamental frequency, for an acoustic level of 70 dB. However, the level at twice that frequency is overestimated. A possible explanation for this discrepancy is the simplification made of a constant spinning rate in the computations: the variations of the spinning rate over one revolution are not taken into account to derive the expression of unsteady aerodynamic forces and moment. As a consequence, a part of the non-linearity leading to the generation of higher harmonics from the fundamental frequency is ignored. The third peak frequency is under-estimated, which is a consequence of having neglected the higher-order Fourier components in the approximation of the CFD results. Furthermore, the sub-harmonics are not reproduced, again due to the approximations. Since the first two peaks dominate the spectrum by at least 25 dB, ignoring the aforementioned details is not detrimental to the application. The overall agreement partially validates the simulation code.

The aero-mechanical and acoustical simulation of a complete bullroarer, including the effect of the string return torque, has been performed in a second step. The results are better emphasized by looking directly at the typical time-frequency analysis of Figure 17, as computed in the same conditions as in Figure 2. The following features are observed, in both the measured and computed signals and maps.

The wave packets in the time signal repeated with a period of about 4 seconds correspond to the reversal of the cone occuring at each spinning inversion half-cycle. At reversal the sound pitch and level almost vanish. The progressive frequency drop is followed by a faster increase. This is an effect of inertia, responsible for a short accelera-

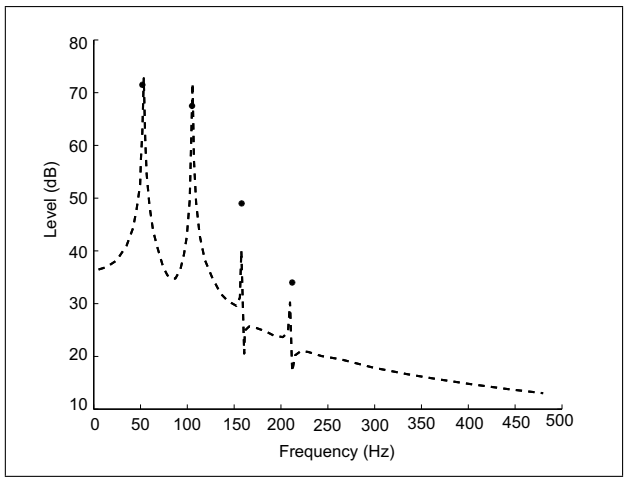

Figure 16. Computed acoustic spectrum. $U_0 = 11$ m/s; $\xi = 0.45$. Same conditions as in the experiment of Figure 13a. Black dots stand for the measured peak values.

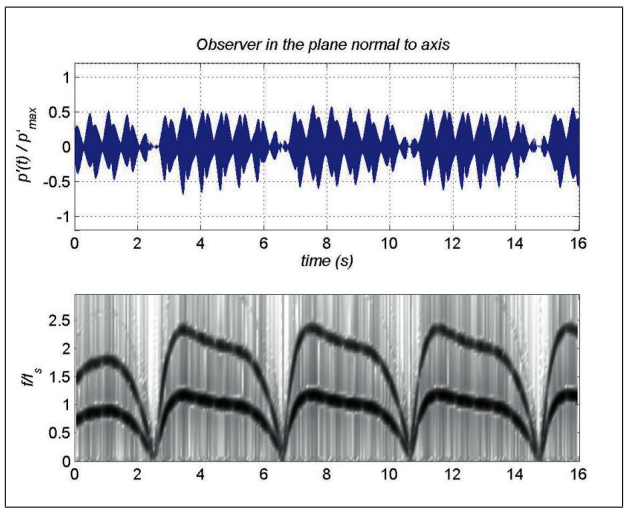

Figure 17. Time-frequency analysis of a bullroarer sound synthesis.

tion at a spinning rate slightly higher than the expected one for autorotation. Then the frequency, as well as the cone angle (not shown here) are roughly stabilized till the next reversal. During this time of relative stabilization, the spinning frequency is close to the natural autorotation value. This value defines the dominant pitch of the bullroarer.

Each revolution around the user's hand is associated with a secondary spot inside a wave packet of the time signal, every half-cycle of inversion including about 6 of them. The corresponding time scale is the whirling period. In the experiment, the spotting can be attributed to the variable effort made by the user to sustain the motion, that cannot be made perfectly regular. In the computation, this does not hold any more and other sources of cyclic variations must be found. The varying source-to-microphone distance inducing amplitude modulations can explain the spotting. The convective amplification accompanying the Doppler effect and involved in equation (7) through the term $(1 - M_r)^2$ could also be mentioned. However, in view of the very small value of the Mach number, this effect cannot be significant here. Lastly the directivity of the slat is to be considered. For an observer location normal to the **Z** axis and a large apex angle of the cone, the observer nearly faces the **z** axis twice per whirling revolution. At the corresponding times, the sound emitted towards the observer must approach zero by virtue of the dipole nature of the equivalent source. This suggests two extinctions, or approximate conditions, every revolution. Such additional subdivisions are clearly noticeabled on every spot in Figure 17, corresponding to the half whirling period thus diametrically opposed locations of the slat with respect to the microphone. The same is already observed in Figure 2, less clearly because of a less regular driving, and especially in the first two wave packets. Finally, the agreement between the measured and computed sounds and the preceding arguments show that the wobbling effect is primarily due to the directivity of the slat and to a minor extent to the variation of relative distance between source and observer. Note that the latter variation would not be a source of modulation any more for a distant observer. By the way, it is clearly understood that the modulations in the sound radiated by a bullroarer are at their maximum amplitude when the observer is at 90° to the **Z** axis, the sound along this axis being more regular.

7. Conclusions

A complete aeromechanical and aeroacoustical theory of the whirling aerophone called bullroarer has been proposed in this paper, together with basic experiments. It has been shown that the motion of a bullroarer is sustained by the combined effect of the autorotation acting on the slat and of the return torque from the string.

Autorotation of a slat with thin elliptical cross-section has been characterized both from the aerodynamical and acoustical points of view. The key feature of the flow is a single autorotation vortex attached to the retreating edge of the slat. The dynamics of this vortex induces fluctuations of drag and lift forces, acting as compact acoustic dipoles. Normal autorotation conditions correspond to a constant velocity parameter, defined as the tangential velocity of the slat edges divided by the relative lateral flow on the slat. In other words, the spinning rate is proportional to the whirling frequency imposed by the user. As a result, the fundamental pitch of a bullroarer is proportional to the whirling frequency and the inverse chord length. In that case, as expected from classical dimensional analysis in aeroacoustics, the acoustic intensity scales like the sixth-power of the flow velocity or the whirling frequency. Some additional results confirm that autorotation noise is a rapidly increasing function of the velocity parameter, for fixed oncoming flow velocity or whirl. The fundamental frequency of the sound is twice the spinning frequency; however, both the free autorotative motion and the usual running of a bullroarer exhibit a weak sub-harmonic behaviour, mainly attributed to the non linearity in the au-

torotation phenomenon, and not deeply investigated in this paper.

A simulation code, using simple formulae deduced from interpolated CFD results for the description of the aerodynamic forces and moment, and solving the equations of mechanics by a standard technique in the time domain, allowed computation of the sound in the far field. The results are in very good agreement with experimental observation, both in the case of a spinning slat in a wind-tunnel and the case of a real bullroarer. The code can be used to provide a realistic sound synthesis.

Acknowledgement

The authors are grateful to John Davis of the Australian Music Center NSW and to Michèle Castellengo of the Laboratoire d'Acoustique Musicale, University of Paris VI, for providing recording references.

References

[1] M. Atherton: Australian made ... australian played. New South Wales University Press, 1990. Also audio compact disc OZM 1008.

[2] Unesco Collection: Musics and musicians of the world. Brazil: the Bororo world of sound. Compact disc D 8201, AD 090.

[3] A. Schaeffner: Origine des instruments de musique. Johnson reprint corp., 1936.

[4] S. Sadie: The new grove dictionary of musical instruments. McMillan Press Ltd, 1984. 283-284.

[5] J. E. Ffowcs Williams, D. L. Hawkings: Sound generation by turbulence and surfaces in arbitrary motion. Phil. Trans. Roy. Soc. A **264** (1969).

[6] M. Roger, S. Aubert: Autorotation and the theory of bullroarer sound. 5th AIAA/CEAS Aeroacoustics Conference, Seattle WA, 1999, paper no.99–1827.

[7] N. H. Fletcher, A. Z. Tarnopolsky, J. C. S. Lai: Rotational aerophones. J. Acoust. Soc. Amer. **111** (2002) 1189–1196.

[8] G. K. Batchelor: An introduction to fluid dynamics. Cambridge Univ. Press, 1967.

[9] M. E. Goldstein: Aeroacoustics. McGraw-Hill book company, 1976.

[10] M. J. Lighthill: On sound generated aerodynamically 1: General theory. Proc. Roy. Soc. A **221** (1952).

[11] M. V. Lowson: The sound field for singularities in motion. Proc. Roy. Soc. A **286** (1965).

[12] D. Casalino: An advanced time approach for acoustic analogy prediction. J. Sound Vib. **261** (2003) 583–612.

[13] S. Aubert, P. Ferrand: Study of unsteady transonic flows with a new mixed van leer flux splitting method. – In: 7th International Symposium on Unsteady Aerodynamics and Aeroelasticity of Turbomachines. Tanida, Namba (eds.). Elsevier, 1994, 23–38.

[14] S. Aubert, L. Hallo, P. Ferrand, M. Buffat: Numerical behavior of unsteady waves. AIAA Journal **33** (1995) 888–893.

[15] C. A. J. Fletcher: Computational techniques for fluid dynamics. – In: Series in Comp. Physics. Springer Verlag, Berlin, 1991.

[16] F. N. M. Brown: See the wind blow. University of Notre-Dame, Indiana, 1971.

[17] J. D. Iversen: Autorotating flat-pate wings: the effect of the moment of inertia, geometry and Reynolds number. J. Fluid Mech. **92** (1979).

[18] R. D. Blevins: Applied fluid dynamics handbook. Van Nostrand Reinhold Company, 1984.

[19] R. Comolet: Mécanique des fluides expérimentale. Tome II: Dynamique des fluides réels et turbomachines. Masson, Paris, 1982.

[20] H. J. Lugt: Autorotation of an elliptic cylinder about an axis perpendicular to the flow. J. Fluid Mech. **99** (1980).

[21] H. J. Lugt, S. Ohring: Rotating elliptic cylinders in a viscous fluid at rest or in a parallel stream. J. Fluid Mech. **79** (1977).

[22] H. J. Lugt: Autorotation. Ann. Rev. Fluid Mech. **15** (1983).

[23] D. Casalino: Analytical and numerical methods in vortex-body aeroacoustics. Thèse École Centrale de Lyon 2002-13, 2002.